Characteristics and Profile Asymmetry Properties of Waves Breaking over an Impermeable Submerged Reef

Mayilvahanan Alagan Chella[1]*, Hans Bihs[1], Dag Myrhaug[2]
[1]Department of Civil and Environmental Engineering
[2]Department of Marine Technology
Norwegian University of Science and Technology (NTNU), 7491 Trondheim, Norway

Coastal Engineering, 2015, **100** , pp. 26-36.

Abstract

In the present study, a 3D two-phase flow CFD model that solves the unsteady, incompressible Reynolds-Averaged Navier-Stokes equations has been used to simulate breaking waves over a submerged reef. The level set method is used to capture the complex free surface and the turbulence is described by the $k-\omega$ turbulence model. The numerical model was evaluated by comparing the computed results with the experimental data by Blenkinsopp and Chaplin (2008) and the computed results are in good agreement with the measured data. The computed results over the submerged reef clearly depict the flow features associated with the breaking process such as the complex interface deformation, the formation of the plunger vortex and the downstream vortex, the splash-up phenomenon and the movement of the enclosed air pocket. The main aim of the study was to investigate the effect of the offshore wave steepness and the water depth above the reef crest on the characteristics and the profile asymmetric properties of waves breaking over a submerged reef. The computed results suggest that the water depth over the reef crest affects the prominent characteristics of waves breaking over a reef such as breaker type, water depth at breaking, breaker indices and geometric properties.

Keywords:

Breaking waves, profile asymmetry properties, numerical modeling, breaker indices, submerged reef

*Corresponding author, mayilvahanan.a.chella@ntnu.no
Postprint, published in Coastal Engineering, doi: http://dx.doi.org//10.1016/j.coastaleng.2015.03.008

1 Introduction

Wave breaking is a prominent research subject in coastal and marine engineering. It is a two phase flow phenomenon involving air and water, and it strongly influences the air-sea interaction by enhancing mass, momentum and energy transfer between the phases. It thereby limits the wave steepness, generating vorticity and turbulence, enhancing wave energy dissipation, entraining air and white water formation. Despite a considerable number of experimental, numerical and theoretical studies and field observations have been carried out to investigate the process, the wave breaking mechanism is not completely understood. A comprehensive examination of breaking wave properties is inevitable to understand the mechanism of wave breaking and thus the description of the breaking process. Wave breaking over a submerged reef primarily depends on the tidal level and the characteristics of the incident waves. Moreover, an accurate description of waves breaking over submerged structures has always been a central issue in estimation of hydrodynamic loads on marine structures. Numerous studies

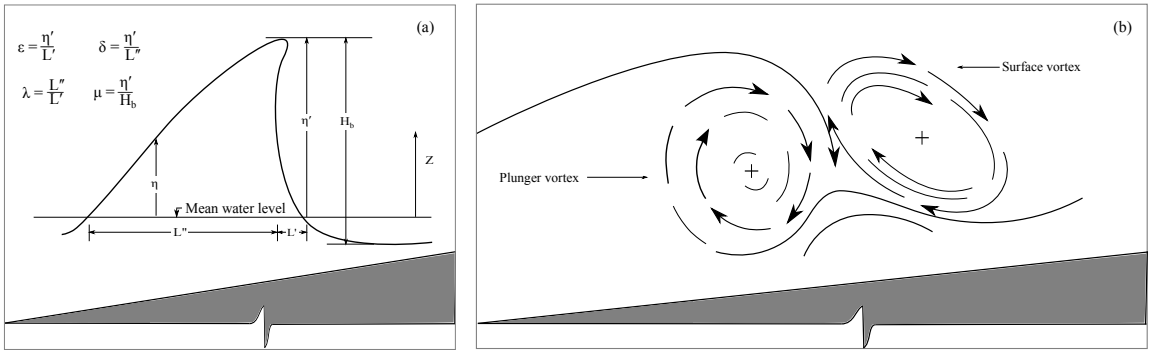

Figure 1: (a) Definition sketch of local wave profile asymmetry parameters following Kjeldsen and Myrhaug (1978) and (b) Schematic of generation of plunger vortex and surface roller during breaking following Basco (1985)

.

have attempted to explain the wave breaking process and their characteristics, and a detailed literature review on wave breaking in deep and shallow water can be found in Cokelet (1977); Peregrine (1983); Basco (1985); Banner and Peregrine (1993); Perlin et al. (2013). The characteristics of wave breaking over slopes are strongly affected by the local environmental parameters, water depth (d), offshore wave steepness (H_0/L_0) and sea bed slope (m). On plane slopes, the offshore wave steepness and seabed slope determine the breaker characteristics (Iversen, 1952; Galvin, 1968; Battjes, 1974). In the case of a submerged reef, however, wave breaking is strongly influenced by the water depth and the wave height at the crest of the reef. This has been studied in laboratory experiments by Gourlay (1994); Smith and Kraus (1990); Blenkinsopp and Chaplin (2008); Yao et al. (2013). They suggested that the application of the surf similarity parameter proposed by Battjes (1974) is inappropriate to categorize the breaker type of waves breaking over submerged structures. Several studies on submerged breakwaters have revealed the role of the water depth at the reef crest and the offshore wave height on the wave transformation properties (Ahrens, 1987; Ting and Kim, 1994; Iwata et al., 1996; Kawasaki and Iwata, 1998). Hence, the wave breaking process over

a submerged reef with a fixed crest height is very sensitive to the water depth and the wave height at the crest. During the course of the tidal cycles, the water depth over a submerged reef continuously changes, which has a substantial impact on the wave breaking process and its characteristics. Blenkinsopp and Chaplin (2008) performed a series of experiments to investigate the effect of the water level on the characteristics of the breaking process over a submerged reef with a slope of 1/10. They found that, although the water level does not strongly affect the breaker indices unlike on plane slopes, it influences the breaker type, reflection and transmission characteristics. However, a relationship exists between the asymmetric parameters and the breaker type and this has been first reported by Kjeldsen and Myrhaug (1978). They introduced steepness and asymmetry parameters to define the asymmetry of the wave profile: crest front steepness (ε), crest rear steepness (δ), the vertical asymmetry factor (λ) and the horizontal asymmetry factor (μ) as depicted in Fig. 1 (a). Additionally, the geometric properties of breaking waves can be related to the breaker type, which plays a key role in estimation of breaking wave forces on marine structures (Alagan Chella, M. and Tørum, A. and Myrhaug, D., 2012). Importantly, the breaker shape influences the size and strength of the breaker vortices. Research has been reported on the geometric parameters of breaking waves in deep water (Kjeldsen and Myrhaug, 1978; Bonmarin, 1989; Lader, 2002; Babanin et al., 2010) and in shallow water (Ippen and Kulin, 1954; Miller and Zeigler, 1964; Adeyemo, 1968; Iwagaki and Sakai, 1972).

Several surface wave theories can only be applied to describe the waves with small fluid accelerations compared to gravity such as Airy's and Stokes theory based on small wave steepness approximations, solitary and cnoidal wave theories based on the nonlinear shallow water equations and the Korteweg-De Vries equations (Babanin, 2011). Longuet-Higgins and Cokelet (1976) first proposed a boundary element method based on two dimensional potential theory and conformal mapping to model periodic breaking waves in deep water. Later the method was modified by Vinje and Brevig (1981), using the physical plane representation to finite water depth. The main flow features of wave transformation over submerged structures are the creation of higher harmonics and vortices. It is possible to model the breaking process using the potential theory prior to the water jet impingement on the water surface by the breaker (Chen et al., 1999; Christensen, 1998). Most studies in the field of submerged breakwater structures have only focused on the prediction of the reflection and transmission characteristics of waves for a given environmental condition. The theoretical and numerical description of the flow problem was based on potential theory which does not account for the rotational flow. Ting and Kim (1994) investigated the wave transformation over a submerged structure and concluded that potential theory cannot be applied to model the flow process such as flow separation and energy dissipation. However, the generation and dissipation of vortices during the breaking process are created by rotational flow (not potential) (Takikawa and Yamada, 1997). In addition to that, viscous fluid forces and associated turbulence become significant during the wave breaking process.

Moreover, measures of incipient breaking of regular waves such as geometric, kinematic and dynamic breaking criteria are connected to the limiting value of wave steepness, horizontal fluid velocity and downward vertical acceleration, respectively. Much uncertainty still exists in defining incipient breaking and breaking onset. Importantly, these criteria are a function of many physical parameters and comprehensive measurements are relatively limited and are still challenging to obtain. Some of the indirect analytical approaches, such as the Boussinesq approximation, are based on the interpretation of the energy dissipation due

to breaking with pre-breaking and post-breaking wave properties and cannot describe the breaking process completely (Babanin, 2011). Numerical modeling of wave breaking becomes challenging due to the intricacy in describing the physical processes involved such as air-sea interaction, vorticity generation, overturning motion, the air entrainment etc. A straightforward approach to describe the breaking process numerically is to solve the fundamental fluid dynamic equations with Computational Fluid Dynamics (CFD). The method is able to capture the prominent flow properties during breaking without specifying breaking criteria or relying on empirical criteria. CFD models that are based on a single-phase flow which concerns only liquid flow and disregards the air phase during breaking have been presented by e.g. Lin and Liu (1998), Bradford (2000) and Zhao et al. (2004). Computational studies of the breaking process with two-phase flow CFD models has gained much attention in recent years by Chen et al. (1999); Christensen and Deigaard (2001); Hieu et al. (2004); Christensen (2006); Wang et al. (2009*a*,*b*); Bakhtyar et al. (2013); Jacobsen et al. (2012). Two-phase flow CFD models account for the interaction of air above the free surface, density difference at the interface and entrapped air during breaking.

The main objective of the present numerical study is to investigate the effects of offshore wave steepness and water depth on the characteristics and geometry properties of waves breaking over a submerged reef. A three-dimensional (3D) numerical wave tank based on two-phase flow CFD model is used in a two-dimensional (2D) setup to model waves breaking over a submerged reef. The present numerical model is validated by comparing the numerical results to experimental data by Blenkinsopp and Chaplin (2008), and the computed results agree well with the experimental data. The wave breaking characteristics such as the incipient breaker height and water depth at breaking, incipient breaker indices and wave profile asymmetry properties are investigated in detail to understand the physical features associated with the breaking process. Moreover, the present numerical investigation is limited to the wave transformation up to the inner breaking region (Svendsen et al., 1978).

2 Computational method

2.1 Governing Equations

In the present 3D numerical model, the incompressible Reynolds-Averaged Navier-Stokes equations are used to describe the two-phase viscous flow. The governing equations are:

$$\frac{\partial U_i}{\partial x_i} = 0 \tag{1}$$

$$\frac{\partial U_i}{\partial t} + U_j \frac{\partial U_i}{\partial x_j} = -\frac{1}{\rho}\frac{\partial P}{\partial x_i} + \frac{\partial}{\partial x_j}\left[(\nu + \nu_t)\left(\frac{\partial U_i}{\partial x_j} + \frac{\partial U_j}{\partial x_i}\right)\right] + g_i \tag{2}$$

U is the velocity averaged over time t, ρ is the fluid density, P is the pressure, ν is the kinematic viscosity, ν_t is the eddy viscosity and g the gravity term. Since the numerical model is used as a numerical wave tank, higher order schemes are employed to avoid the unphysical excessive damping of free surface waves. The discretization of the convection term of the RANS equations is accomplished by the 5-th order Weighted Essentially Non-Oscillatory (WENO) scheme in the conservative finite difference version (Jiang and Shu, 1996). This WENO scheme consists of three substensils that are weighted based on the local smoothness

of the discretised function. Moreover, this scheme provides very robust numerical stability without causing numerical oscillations.

Time discretization is performed with a third-order accurate total variation diminishing (TVD) Runge-Kutta scheme consisting of three Euler substeps (Shu and Osher, 1988). The velocities at each Euler substep are obtained by solving the pressure term with the projection method. The BiCGStab algorithm (van der Vorst H., 1992) with Jacobi preconditioning calculates the pressure from the Poisson equation. It is well known that a large amount of wave energy is dissipated as turbulence in the free surface layer during the breaking process. The turbulence is modeled with the RANS equations coupled with the $k-\omega$ model. A ghost-cell immersed boundary method based upon the local directional by Berthelsen and Faltinsen (2008) is employed to account for the solid boundaries of the fluid domain. In addition to that, complex geometries can be represented without specifying the boundary conditions explicitly.

2.2 Free surface

One of the major challenges in the modeling of the breaking process is to describe the free surface changes i.e. interface deformation. Here, the level set method (Osher and Sethian, 1988) is chosen since the free surface changes can be obtained without any special treatments at the interface. The level set method is an Eulerian method and represents the interface between the two phases water and air. The interface is the zero level set of the smooth signed distance function $\phi(\vec{x},t)$. At any point on the computational domain, the level set function gives the distance from the interface and the sign of the function marks the fluid phase as follows:

$$\phi(\vec{x},t)\begin{cases} > 0 \; if \; \vec{x} \in water \\ = 0 \; if \; \vec{x} \in \Gamma \\ < 0 \; if \; \vec{x} \in air \end{cases} \tag{3}$$

Also the Eikonal equation $|\nabla\phi| = 1$ is valid. When the interface is moved under an externally generated velocity field $\vec{v}$, a convection equation for the level set function is obtained:

$$\frac{\partial\phi}{\partial t} + U_j\frac{\partial\phi}{\partial x_j} = 0 \tag{4}$$

The fluid properties such as the density ρ and the viscosity ν can be defined for the computational domain with the level set method. However, the discontinuity in the fluid properties across the interface can cause numerical instabilities in the solution. This discontinuity is removed by smoothing the fluid properties over a small distance in the region close to the interface with a Heaviside function $H(\phi)$. This region is 2ϵ thick, with ϵ being proportional to the grid spacing dx. The density and the viscosity from the level set function can be written as:

$$\begin{aligned} \rho(\phi) &= \rho_{water}H(\phi) + \rho_{air}(1 - H(\phi)), \\ \nu(\phi) &= \nu_{water}H(\phi) + \nu_{air}(1 - H(\phi)) \end{aligned} \tag{5}$$

and the Heavyside function:

$$H(\phi) = \begin{cases} 0 & if\ \phi < -\epsilon \\ \frac{1}{2}\left(1 + \frac{\phi}{\epsilon} + \frac{1}{\Pi} sin\left(\frac{\Pi\phi}{\epsilon}\right)\right) & if\ |\phi| < \epsilon \\ 1 & if\ \phi > \epsilon \end{cases} \quad (6)$$

2.3 Numerical wave generation and absorption

The present numerical model is used as a numerical wave tank. Wave generation is performed at the inflow boundary and waves are absorbed at the outflow boundary using the relaxation method presented by Larsen and Dancy (1983). With the relaxation method, reflected waves from the reef face are absorbed at the inlet boundary of the wave tank. If a nonlinear analytical solution is known, it can be used as the imposed solution to moderate the computational solution. This is a relatively straightforward approach for the wave generation in a numerical wave tank and proves to be efficient, as this has been presented by Mayer et al. (1998), Engsig-Karup (2006) and Jacobsen et al. (2012). Waves are absorbed at the outlet boundary with a relaxation zone where the velocity components are gradually reduced to zero and the water surface and the pressure follows the hydrostatic distribution at the still water level.

3 Computational domain, cases and parameters

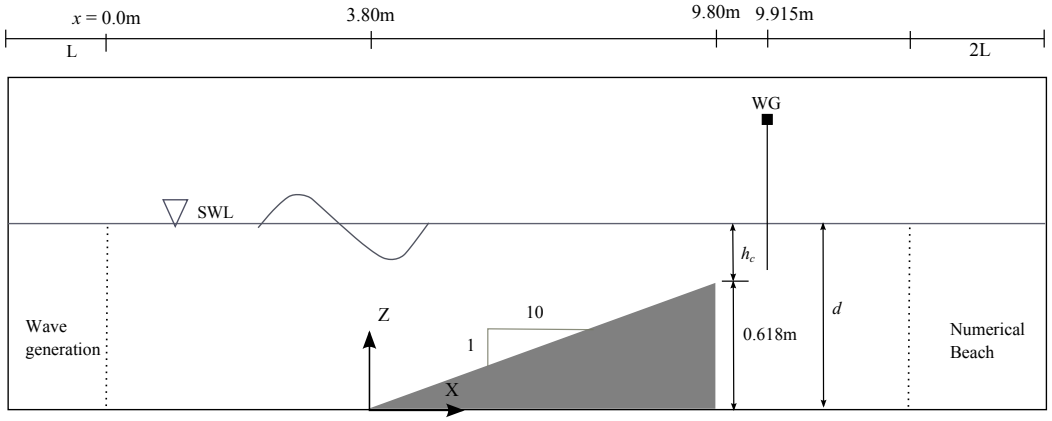

Figure 2: Computational domain

In order to validate the present numerical model, the numerical results are compared with the experimental data measured by Blenkinsopp and Chaplin (2008). The numerical wave tank consists of a submerged reef with a height of 0.62m and a slope of 1/10, located 3.8m from the wave generation zone as shown in Fig. 2. The numerical set-up, incident wave parameters and the coordinate system are the same as the experimental conditions presented in Blenkinsopp and Chaplin (2008). The computed results of two experiment cases with different reef crest submergences, h_c=0.032m and 0.102m (d=0.65m and 0.72m) are compared to the experimental measurements. The free surface elevations are obtained using a wave gauge 0.115m after the crest of the reef. The computational domain is discretized with

a uniform grid size in both directions x and y. In the numerical simulations, five waves are generated for each run.

Simulation cases	Simulation no.	Offshore wave steepness, H_0/L_0	Reference water depth, d (m)
Based on offshore wave steepness (H_0/L_0): Case (A)	1 2 3 4 5 6	0.02 0.03 0.04 0.05 0.06 0.07	0.7
Based on reference water depth (d): Case (B)	7 8 9 10 11 12	0.033	0.65 0.68 0.69 0.70 0.71 0.72

Table 1: List of computational cases

The present numerical cases explore the breaking characteristics and geometric properties of waves breaking over the submerged reef and their dependence on offshore wave steepness, (H_0/L_0, H_0 and L_0 are deep water wave height and wave length, respectively, case A) and water depth (d, case B) as listed in Table 1. Case A tests six different offshore wave steepnesses ranging from 0.02 to 0.07 at a fixed water depth, and case B examines a wave with a fixed offshore wave steepness of 0.033 at six different water depths from 0.65m to 0.72m.

Most of the previous studies have been conducted to establish relationships between the characteristics of waves at the breaking point. The breaking point is assessed in the present study as the point where part of the wave front becomes vertical. Thus, the computed water depth (d_b) and wave height (H_b) at the breaking point are used to calculate the breaker indices. The breaker depth index, γ_b, is the ratio of the breaker height H_b to the water depth at breaking d_b:

$$\gamma_b = \frac{H_b}{d_b} \tag{7}$$

The breaker height index, Ω_b is the ratio of the breaker height H_b to offshore wave height H_0:

$$\Omega_b = \frac{H_b}{H_0} \tag{8}$$

It is well known that the wave profile becomes asymmetric as it approaches the breaking point and cannot be described by the wave steepness (H/L). Hence, additional parameters are required to describe the asymmetric shape of the wave at breaking. Four additional geometric parameters proposed by Kjeldsen and Myrhaug (1978) are used in this study to describe the asymmetry of the wave profile as shown in Fig. 1 (a).

3.1 Grid dependence study

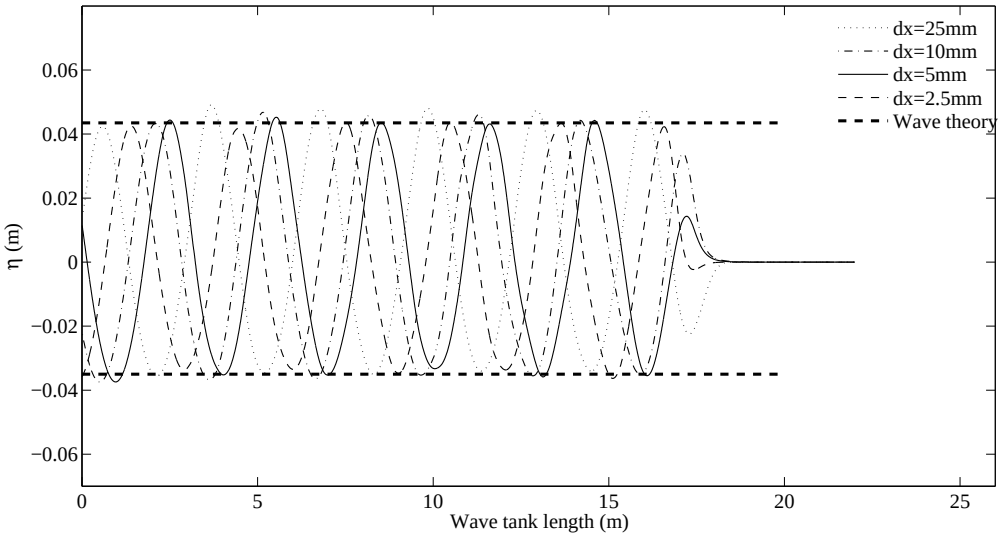

Figure 3: Grid sensitivity study on computed free surface elevations

Since the numerical model uses a uniform Cartesian grid, the computational domain is discretized with a uniform grid size in both directions x and y. In order to investigate the effect of grid sizes (dx) on the simulation results, four different grid sizes, dx= 25mm, 10mm, 5mm and 2.5mm, are examined. Fifth-order Stokes waves with H=0.12m and T=1.5s are simulated in the numerical wave tank without any structure. The free surface elevations for the different grid sizes are compared with the maximum and minimum values of the theoretical result as shown in Fig. 3. It appears that the difference between the numerical results and the theoretical result decreases as the grid size decreases, showing that the wave surface elevations for dx=5mm and 2.5mm, agree well with the theoretical results. However, the grid size dx=2.5mm with 1248 cells per wave length demands more computation time than dx=5mm with 624 cells. Therefore, in order to perform efficient simulations within a reasonable computing time, the grid size dx=5mm is selected for the present study.

4 Results and discussion

4.1 Numerical model evaluation

The computed wave surface elevation of two experimental cases with different water depths are compared with the experimental measurements by Blenkinsopp and Chaplin (2008). Figs. 4 and 5 show the comparison of computed and measured wave surface elevation for the simulation case with d=0.65m and d=0.72m, respectively. The wave surface elevation is computed 0.115m behind the reef crest, which is an inner breaking region of the surf zone as defined in Svendsen et al. (1978). Although the numerical results are in reasonable agreement with the experimental data for both the cases, the computed wave crests are slightly higher

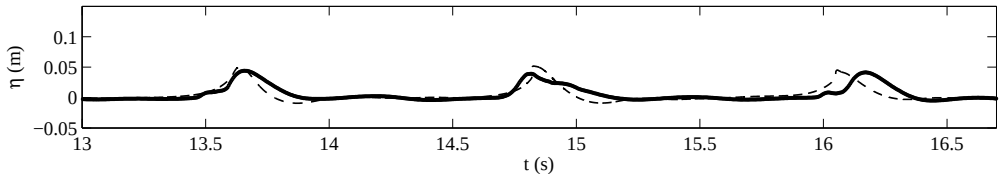

Figure 4: Comparison of simulated and measured wave surface elevation for the numerical case at d=0.65m. Dashed lines: present numerical model; Solid lines: experimental data from Blenkinsopp and Chaplin (2008)

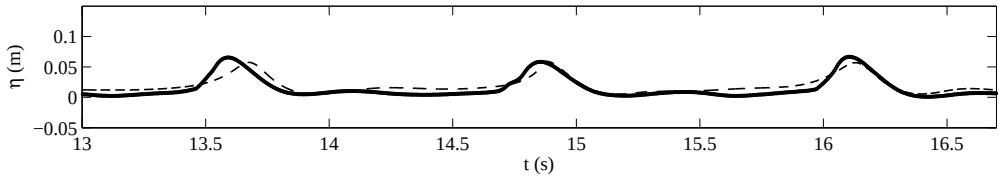

Figure 5: Comparison of simulated and measured wave surface elevation for the numerical case at d=0.72m. Dashed lines: present numerical model; Solid lines: experimental data from Blenkinsopp and Chaplin (2008)

for d=0.65 and slightly lower for d=0.72 than the experimental data. The reason is unclear but this might be related to the energy dissipation in the inner breaking region where the large deterministic flow structures disintegrate into smaller flow structures with extreme chaotic and turbulent behaviour. It is therefore difficult to predict the free surface elevation in this region. However, the present numerical model is capable of calculating the free surface elevation in the inner breaking region with satisfactory accuracy.

4.2 Waves breaking over the reef

The characteristics of waves breaking over a submerged reef solely depend on the wave height and the water depth at the reef crest unlike over a sloping seabed. Hence, the breaker types can not be described by the surf similarity parameter which is more appropriate for plane slopes. During the breaking process, the return flow is created seaward in order to balance the shoreward mass flux created in the overturning wave crest. The interaction between the incoming breaker in the upstream side and the seaward return flow of the preceding wave from the downstream side strongly influences the breaking process and thus the characteristics of breaking waves. This effect has been studied in detail by Smith and Kraus (1990) and Blenkinsopp and Chaplin (2008). It is highly challenging to capture the seaward return flow that is generated during the breaking process experimentally and numerically since the flow pattern becomes complex during the extreme changes in the gross mass flux distribution. The initial evolution of the overturning wave crest also causes drastic changes in the free surface. Moreover, Blenkinsopp and Chaplin (2008) have not measured the return flow in the experimental investigation and therefore, the experimental data is not available to compare against the numerical results.

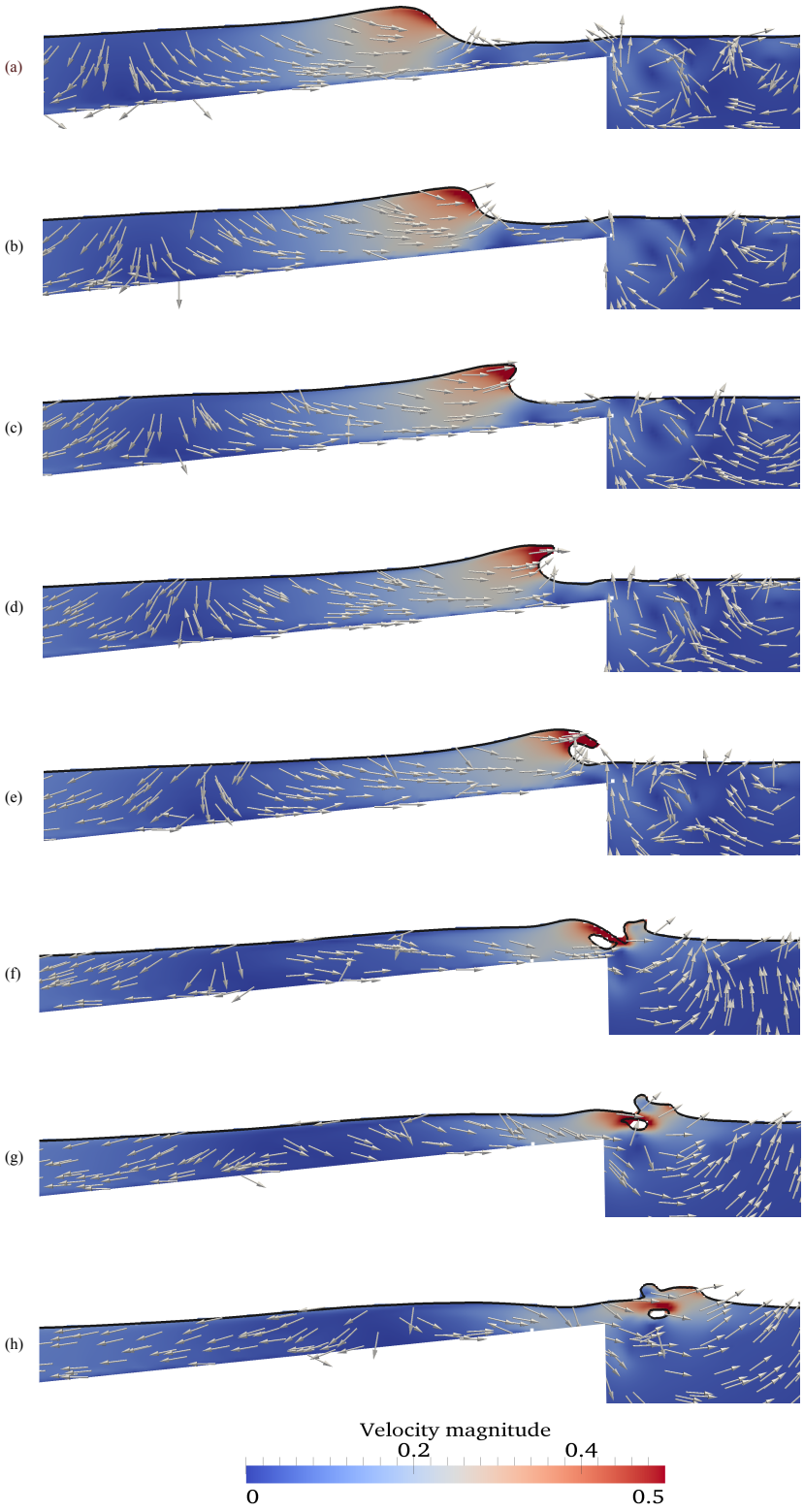

Figure 6: Simulated free surface profile with velocity (m/s) variation during waves breaking over the reef from 9.5s to 9.9s with a time step of 0.05s (a to h) for the simulation case H_0/L_0=0.033 and d=0.65m

Fig. 6 shows the changes in the wave surface profile and the velocity during the breaking process for the wave with H_0/L_0=0.033 at d=0.65m. The wave profile changes with velocity variation during the breaking process clearly depict that a portion of the wave crest with higher velocity moves forward faster than the rest of the wave. Initially, the wave reaches the breaking point as most of the wave front becomes vertical (Fig. 6 (a) and (b)). Then the wave propagates further and the wave crest overturns with an ejecting water jet emanating a plunger vortex as seen in Fig. 6 (c) to (e). When the overturned and ejected wave front hits the free surface at the base of the wave, it almost falls over the wave trough of the preceding wave and generates a surface roller. Then water splashes up causing a rise in the water surface with an air pocket inside the water as shown in Fig. 6 (f) to (h). The two main turbulence zones addressed by Basco (1985) are the toe of the surface roller due to interfacial shear and the outermost part of the plunging vortex as shown in Fig. 1 (b). An extreme changeover from irrotational flow to rotational flow leads to increased vorticity and turbulence as the wave approaches the beach and eventually violent mixing of air and water occurs. It is worth to notice that the impingement of the rotating plunging vortex is causing a secondary wave with new wave characteristics that propagates shoreward as shown in Fig. 6 (f) and (h). Moreover, the numerical prediction of the flow pattern and the wave profile changes are very similar to the observation of the flow features of plunging breakers over plane slopes by Basco (1985).

As Figs. 6 (a) to (e) show, a clockwise vortex is created behind the reef during the breaking process. Initially the size of the vortex is small and it increases as the wave propagates over the reef in order to balance the upstream energy rise in the form of a plunging jet. When the wave trough propagates in the vicinity of the reef crest, the return flow is established around the corner of the reef which opposes the upstream flow. Therefore the wave breaking occurs early further offshore due the combined effect of the reef face friction and the return flow. The vortex further rises up and the size diminishes as the plunger vortex at the wave crest develops. Finally, the downstream vortex weakens and decays rapidly due to the interaction with the plunger vortex upstream. In addition, the down stream vortex size becomes larger as the water depth over the reef crest is increased. This is consistent with those of Iwata et al. (1996); Ting and Kim (1994); Chang et al. (2005) who reported the return flow due to the vortex formation behind the submerged structures. Hence, the numerical model is able to capture the complex interface changes and flow features during breaking process with reasonable accuracy. However, it should be noted that the details of the flow need to be verified against data in order to check the validity of the simulations.

4.3 Characteristics of waves breaking over the reef

The breaking characteristics such as breaker water depth, breaker depth index and breaker height index are examined for different offshore wave steepnesses (case A) and different water depths (case B) as listed in the Table 1.

4.3.1 Incipient wave breaking

Fig. 7 shows the non-dimensional breaker depth (d_b/d) versus the offshore wave steepness (H_0/L_0) and the relative water depth (h_c/d). It appears that d_b/d increases with increasing H_0/L_0 and increasing h_c/d. Therefore, waves over the reef break further offshore at larger

water depth (d_b) as H_0/L_0 and h_c become larger, corresponding to H_0/L_0=0.07 (case A6), d_b/d=0.216 and h_c/d_0=0.14 (case B6), d_b/d=0.14 in Fig. 7. This means that waves with larger H_0/L_0 reaches the breaking point sooner with smaller crest deformation than waves with lower H_0/L_0, which follows the same trend of results on plane slopes. But the crest submergence (h_c) strongly affects the breaker depth (d_b). This suggests that waves propagating over the submerged reef with larger h_c experience more partial reflections, return flow and break further offshore at larger d_b. This also agrees with the experimental observation by Blenkinsopp and Chaplin (2008) and the theoretical study by Battjes (1974). Moreover, the present results appear to be different from the behavior of waves over plane slopes (Rattanapitikon and Shibayama, 2006) and submerged breakwaters (Kawasaki and Iwata, 1998), where d_b decreases as the water depth increases. It seems possible that waves breaking over the submerged reef are strongly influenced by the return flow due to the downstream clockwise vortex, which continues to grow with increasing water depth over the reef crest as presented in Section 4.2. Therefore, waves break further offshore as the reef crest submergence increases.

4.3.2 Breaker depth index (γ_b) and breaker height index (Ω_b)

Fig. 8 presents the comparison of the computed and the measured breaker depth index (γ_b) for different offshore wave steepnesses (H_0/L_0). It appears that γ_b decreases with increasing H_0/L_0, although the experimental data by Blenkinsopp and Chaplin (2008) do not vary much versus H_0/L_0. However, the computed results are in good agreement with experimental data for H_0/L_0 in the range 0.03 to 0.06. In particular, the computed results are slightly higher and

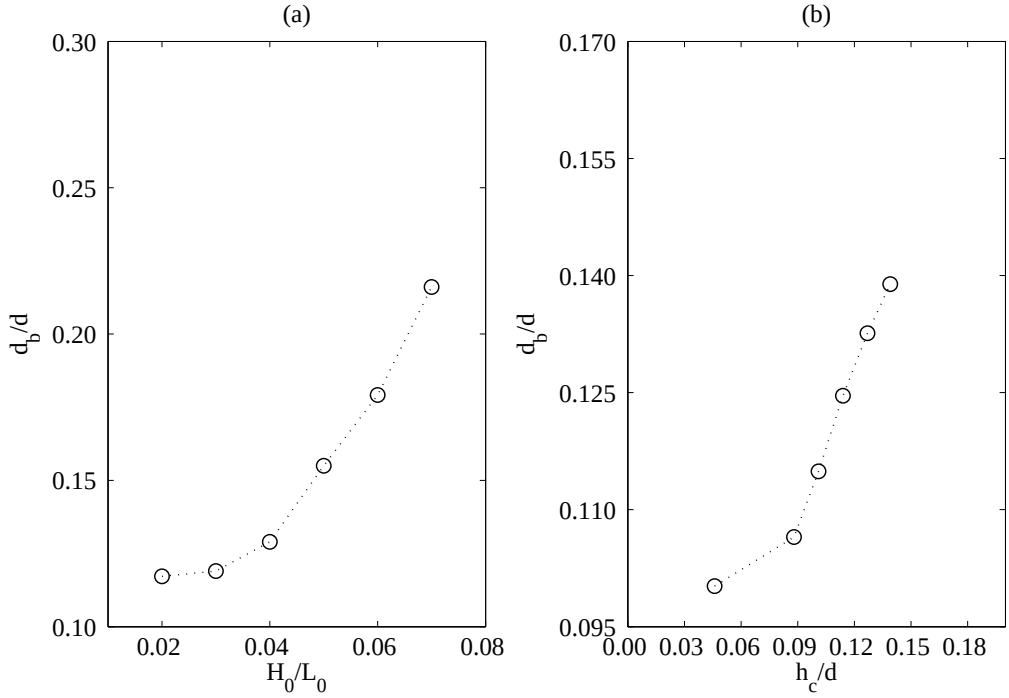

Figure 7: Simulated relative water depth at breaking (d_b/d) as a function of (a) offshore wave steepness (H_0/L_0) and (b) relative water depth (h_c/d)

slightly lower than the experimental results for H_0/L_0 <0.03 and H_0/L_0 >0.06, respectively. Moreover, the numerical prediction follows the experimental trend for waves breaking on plane slopes of 1/10 reported by Smith and Kraus (1990). Fig. 9 shows the comparison of the computed and measured breaker depth index (γ_b) for different relative crest submergence h_c/H_0. It appears that γ_b increases slightly as h_c/H_0 increases for the computations, while γ_b seems to be invariant with h_c/H_0 in the experiments. The computed results are slightly higher and slightly lower than the experiments for $h_c/H_0 > 1.0$ and h_c/H_0 <0.8, respectively. Moreover, the computed results agree well with the experimental data for h_c/H_0 in the range 0.8 to 1.0. It is possible that waves over larger h_c/H_0 break further onshore at higher d_b with larger H_b, corresponding to h_c/H_0=1.143 and γ_b=1.09 (Fig. 9), Ω_b=1.28 (Fig. 12). Fig. 10 presents comparison of the computed and the measured breaker height index (Ω_b) for different offshore wave steepnesses (H_0/L_0), showing that Ω_b decreases as H_0/L_0 increases for both computations and experiments. This is also the case for the Smith and Kraus (1990) experimental results on plane slopes. It appears that the present computations represent an upper bound of the Blenkinsopp and Chaplin (2008) data. Fig. 11 shows the measured reflection coefficient for different offshore wave steepnesses (H_0/L_0) and different relative water depths (h_c/d). It appears that the reflection coefficient (K_r) decreases as H_0/L_0 increases and increases as (h_c/d) increases. This suggests that the wave with small H_0/L_0 experiences more reflections from the reef face, undergoing more deformation during shoaling than the waves with larger H_0/L_0, and reaches the maximum height before it breaks. Similar results have been found by Smith and Kraus (1990); Battjes (1974); Blenkinsopp and Chaplin (2008). Fig. 12 shows comparison of the computed and the measured breaker height index (Ω_b) for

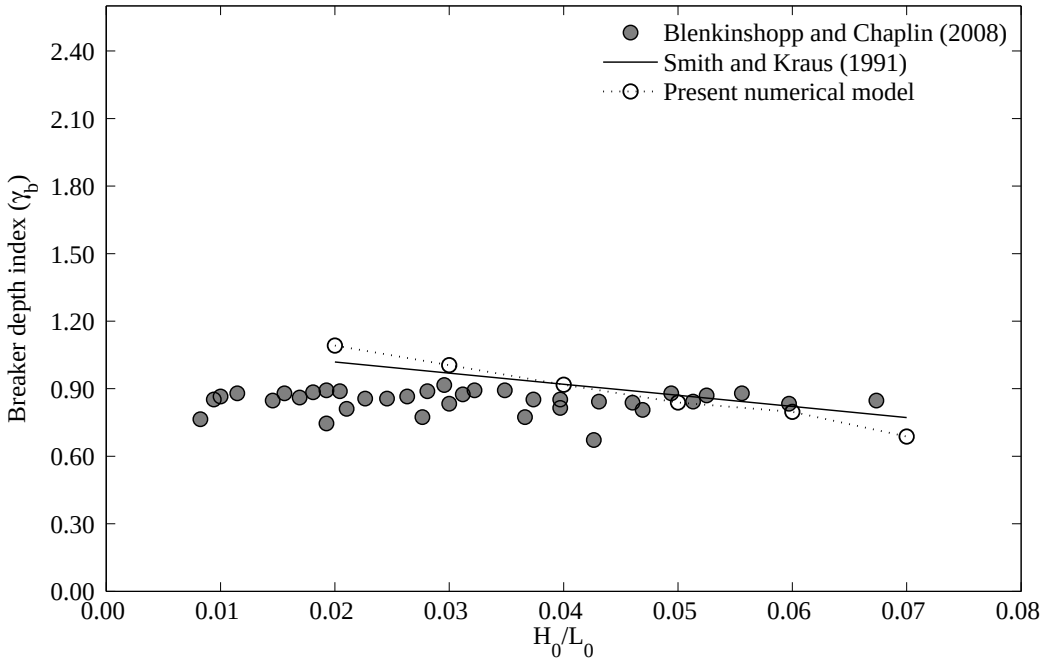

Figure 8: Breaker depth index (γ_b) as a function of offshore wave steepness (H_0/L_0)

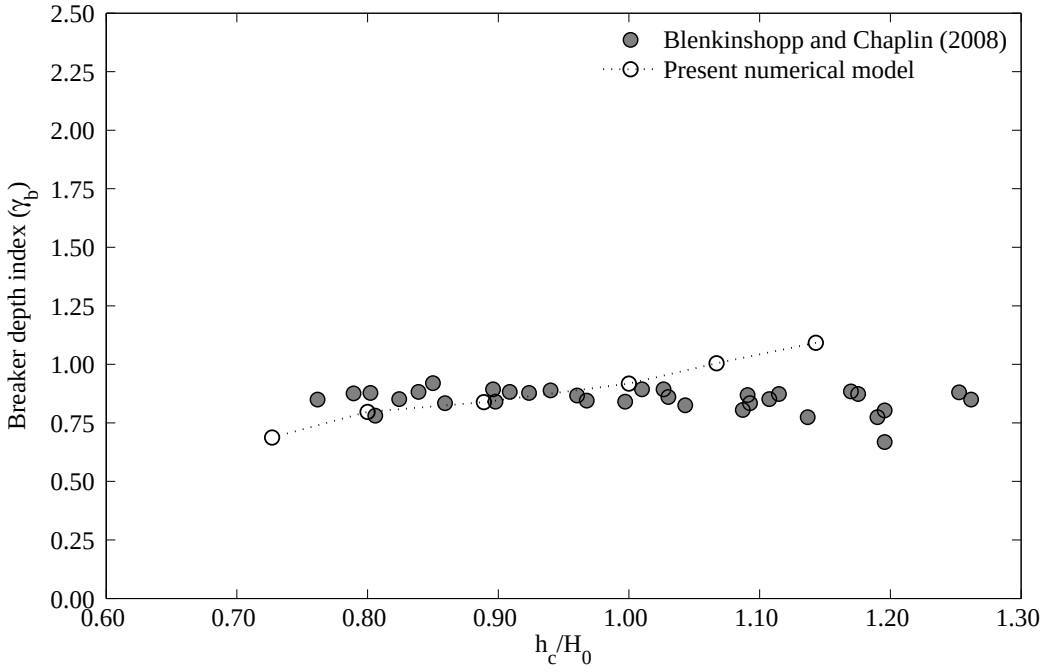

Figure 9: Breaker depth index (γ_b) as a function of relative crest submergence (h_c/H_0)

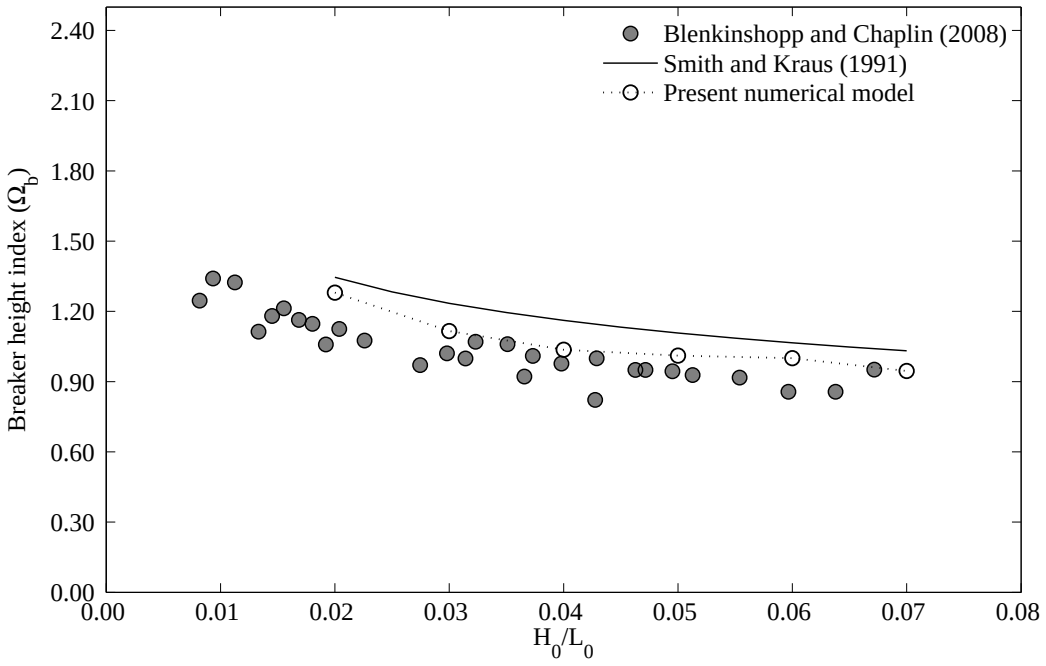

Figure 10: Breaker height index (Ω_b) as a function of offshore wave steepness (H_0/L_0)

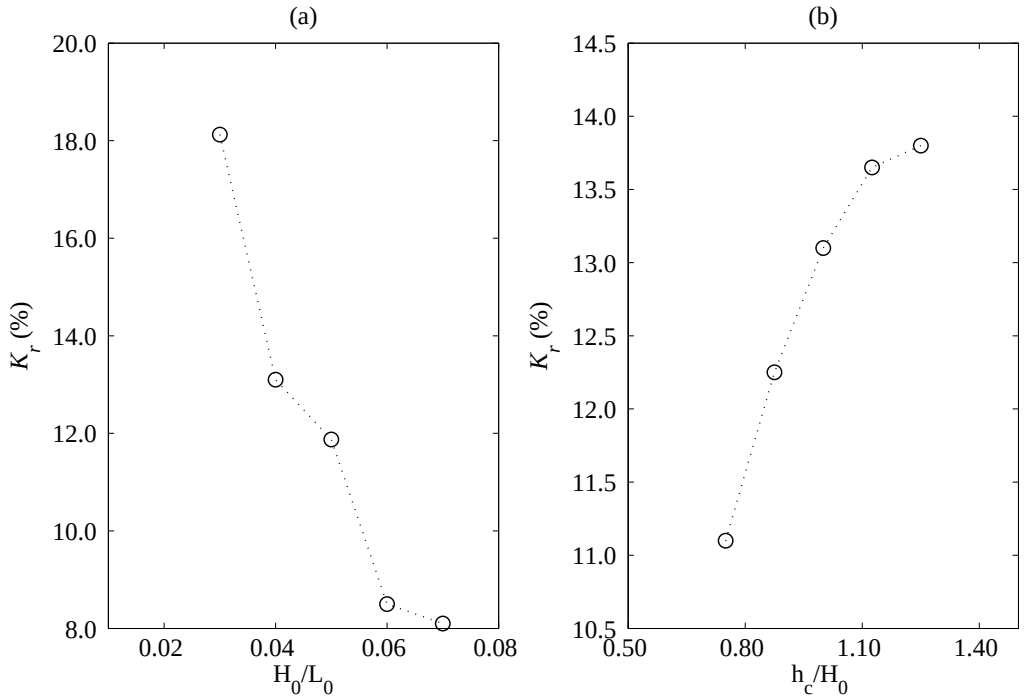

Figure 11: Measured reflection coefficient (K_r) by Blenkinsopp and Chaplin (2008) as a function of (a) offshore wave steepness (H_0/L_0) and (b) relative water depth (h_c/H_0)

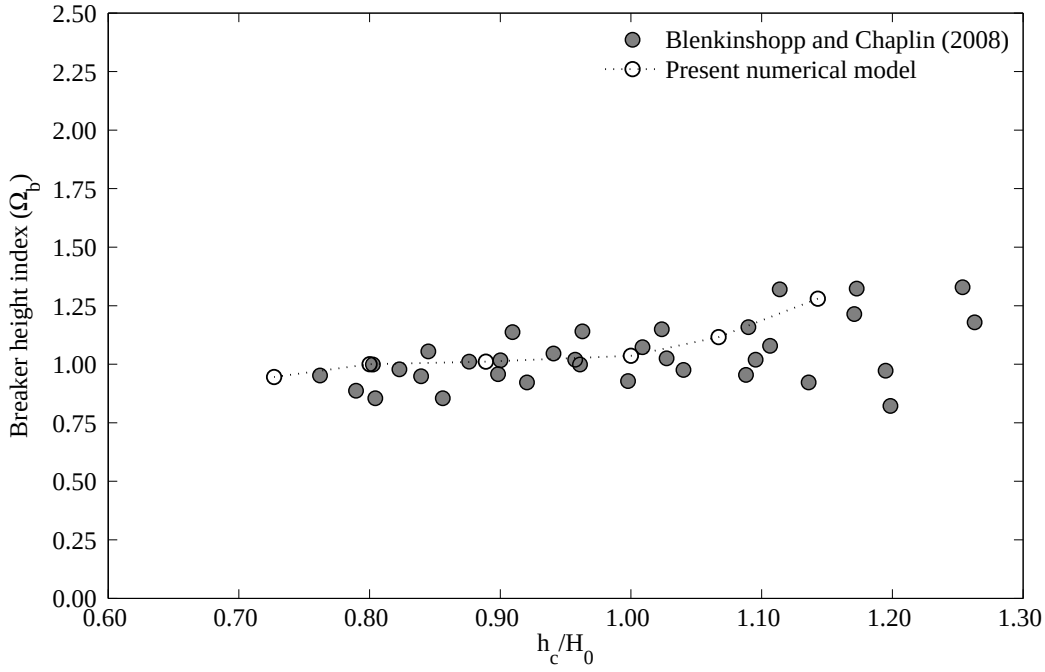

Figure 12: Breaker height index (Ω_b) as a function of relative crest submergence (h_c/H_0)

different relative crest submergence h_c/H_0. It appears that Ω_b increases slightly as h_c/H_0 increases, which agrees well with the experimental data by Blenkinsopp and Chaplin (2008). However, the computed dependence of Ω_b on h_c/H_0 increases slightly more for h_c/H_0 >1.0 than for the experiments. Moreover, Blenkinsopp and Chaplin (2008) reported that there is a strong dependence of reflection coefficient on h_c/H_0. It can be seen from Fig. 11 (b) that the waves propagating over the reef with larger h_c experience more reflection from the reef face. This implies that the waves break at larger d_b with larger H_b, corresponding to h_c/H_0=1.15, Ω_b=1.26 in Fig. 12 and h_c/d=0.14, d_b/d=0.14 in Fig. 7 (b). Fig. 13 shows the breaker

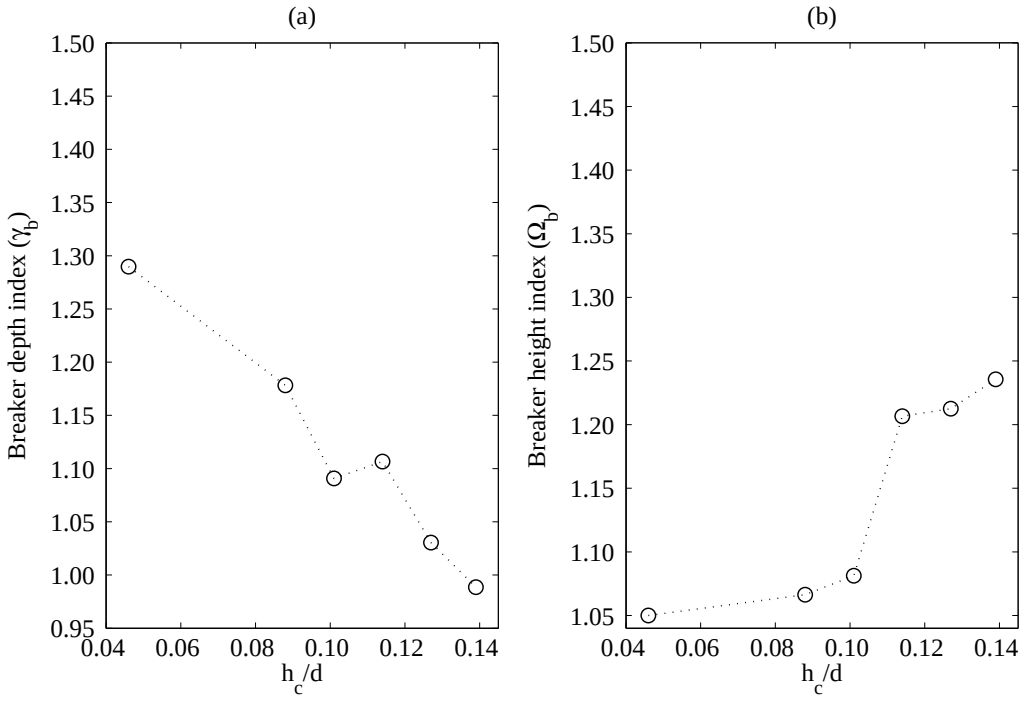

Figure 13: Simulated breaker depth index (γ_b) and breaker height index (Ω_b) as a function of relative depth (h_c/d)

depth index (γ_b) and the breaker height index (Ω_b) versus the relative water depth (h_c/d). It appears that γ_b decreases and Ω_b increases as h_c/d increases. The computed γ_b follows the same trend as observed on plane slopes (Smith and Kraus, 1990; Tsai et al., 2005) but the computed Ω_b is different from the trend on plane slopes. It is seen from Fig. 11 (b) that the value of the reflection coefficient increases as the crest submergence increases. Therefore, the present results suggest that waves advancing over larger h_c break further offshore at higher d_b with larger H_b, corresponding to h_c/d=0.14 and d_b/d=0.14 (Fig. 7 (b)), Ω_b=1.24 (Fig. 9 (b)). In addition to the partial reflection, the return flow due to the vortex formation behind the crest of the reef could also has an influence on the breaking characteristics as mentioned in Section 4.2. It is therefore likely that a moderate relationship may exist between breaker indices and h_c.

4.4 Profile asymmetry parameters

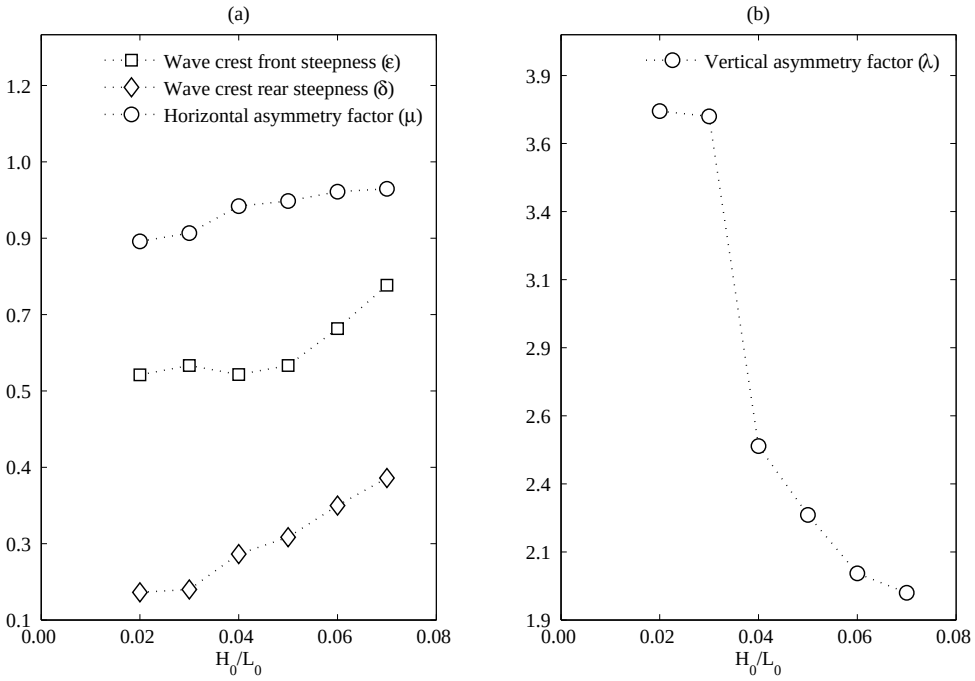

Figure 14: Simulated wave profile asymmetry parameters as a function of offshore wave steepness (H_0/L_0)

Fig. 14 shows the crest front steepness (ε), the crest rear steepness (δ), the horizontal asymmetry factor (μ) and the vertical asymmetry factor (λ) versus the offshore wave steepness (H_0/L_0). It appears that ε, δ, and μ increase and λ decreases for waves with larger H_0/L_0. This suggests that the geometric profile of waves with large values of H_0/L_0 at breaking have a steep wave crest front steepness and wave crest rear steepness and shallower trough without much change in the vertical asymmetry. Meanwhile, waves with lower H_0/L_0 break further onshore with higher crest deformation, corresponding to H_0/L_0=0.02, d_b/d=0.117 in Fig. 7 (a) and H_0/L_0=0.02, Ω_b=1.28 in Fig. 8. Therefore, the breaking wave profile has an ejected wave front with wide rear part without much change in the wave trough and crest front and crest rear steepnesses. It is also observed from Fig. 11 (a) that the effect of reflection is predominant for waves with larger steepness. This deformation is due to the combination of higher partial reflections from the reef face and the slower shoaling process.
Fig. 15 shows the crest front steepness (ε), the crest rear steepness (δ), the horizontal asymmetry factor (μ) and the vertical asymmetry factor (λ) versus the relative water depth (h_c/d). It appears that ε and λ decreases and δ and μ increases with increasing reef crest submergence. As the wave propagates over the reef from the larger d it breaks further seaward with larger breaker height index (Ω_b), corresponding to h_c/d=0.14, d_b/d=0.14 in Fig. 7 (b) and h_c/d=0.14, Ω_b=1.23 in Fig. 13 (b). This implies that the wave profile does not change much from the initial wave shape with a small increase in rear steepness. At the same time, the wave profile becomes more asymmetric when h_c/d decreases.

The wave front becomes steep and ejects forward at the breaking point when h_c/d decreases,

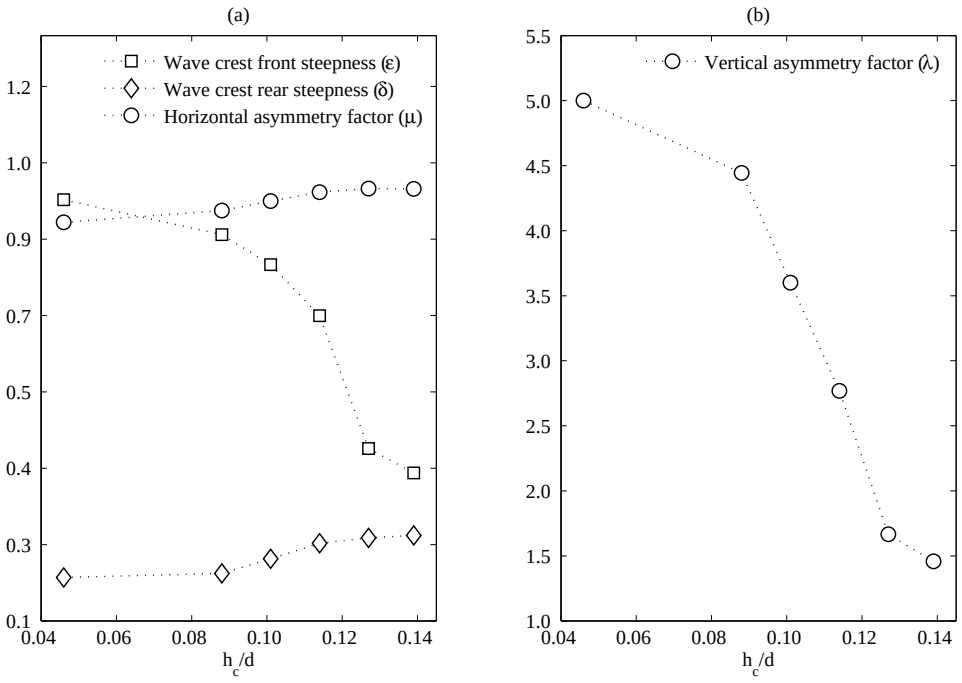

Figure 15: Simulated wave profile asymmetric parameters as a function of relative depth (h_c/d)

which is similar to the development of a plunging breaker. However, for larger values of h_c/d the waves break over the reef as spilling breakers. Moreover, the present results are consistent with those of Sayce et al. (1999) and Blenkinsopp and Chaplin (2008) who state that the breaker type over a submerged reef depends strongly on wave height and water depth.

5 Conclusions

The numerical simulations of waves breaking over a reef have been carried out using a two-phase flow CFD model based on the RANS equation together with the level set method and the $k-\omega$ turbulence model. The computed results show good agreement with the experimental data by Blenkinsopp and Chaplin (2008). It has been shown that the numerical model can provide detailed information about the flow features associated with the breaking process such as the complex interface deformation, formation of plunger vortex and the downstream vortex, the splash-up phenomenon and the movement of the enclosed air pocket. The purpose of the present study was to investigate the effects of offshore wave steepness and water depth on the characteristics and profile asymmetry parameters of waves breaking over a submerged reef. The present work confirms results of previous studies and enhances the understanding of the characteristics and asymmetry properties of waves breaking over the reef. The main conclusions from the numerical study are:

- A clockwise vortex is generated downstream close to the reef crest due to the formation

of a plunger vortex upstream above the reef face. It seems that the downstream vortex is responsible for the return flow.

- The dependence of the offshore wave steepness and the water depth on the breaker water depth is observed. The main factors that affect the wave breaking over the reef are the partial reflection from the reef face and the return flow.
- The computed breaker depth index decreases slightly as the offshore wave steepness increases, and it increases slightly as the water depth above the reef crest increases. For the water depth above the reef crest the most results agree well with those measured by Blenkinsopp and Chaplin (2008), while they found that the breaker depth index was nearly independent of wave steepness.
- The computed breaker height index over the reef matches well with the experimentally measured data and it shows significant dependence on offshore wave steepness and water depth.
- Waves with larger offshore wave steepnesses have a steep wave crest and a shallow trough without much change in the vertical asymmetry, and thus it breaks as a spilling breaker. Waves with small offshore wave steepnesses have an ejected wave front with a wide rear part without significant change in the wave trough and crest front and crest rear steepnesses, and thus it breaks as a plunging breaker.
- A strong dependence of the breaker type on the water depth over the reef crest is clearly observed from the profile asymmetry properties. Waves breaking over the reef have similar features to a plunging breaker for shallower water depth, whereas for a larger water depth waves break similar to a spilling breaker. The degree of asymmetry increases with decreasing water depth above the reef crest.

Acknowledgment

The first author wishes to express his gratitude to late Prof. Geir Moe and late Prof. Alf Tørum for their support. The authors would like to thank Dr. Chris Blenkinsopp and Prof. John Chaplin for sharing the experimental data. The work was supported by the Norwegian Research Center for Offshore Wind Technology (NOWITECH), Research council of Norway (Contract no.193823). The authors would also like to thank NOTUR (Project no. NN9240K) for allocation of computational resources provided on the Vilje system at the super computing facilities at NTNU.

References

Adeyemo, M. (1968). Effect of beach slope and shoaling on wave asymmetry. In: *Proceedings of the 11th conference on Coastal Engineering*, 145–172.

Ahrens, J.P. (1987). Characteristics of reef breakwaters. Technical report, Coastal Engineering Research Center.

Alagan Chella, M. and Tørum, A. and Myrhaug, D. (2012). An overview of wave impact forces on offshore wind turbine substructures. *Energy Procedia*, **20**, 217–226.

Babanin, A.V. (2011). *Breaking and dissipation of ocean surface waves*. Cambridge University Press.

Babanin, A.V., Chalikov, D., Young, I.R. and Savelyev, I. (2010). Numerical and laboratory investigation of breaking of steep two-dimensional waves in deep water. *Journal of Fluid Mechanics*, **644**, 433. ISSN 0022-1120.

Bakhtyar, R., Razmi, A.M., Barry, D.A. and Kees, C.E. (2013). Two-phase flow modeling of the influence of wave shapes and bed slope on nearshore hydrodynamics. *Journal of Coastal Research*, (Special issue 65), 159–164.

Banner, M. and Peregrine, D.H. (1993). Wave breaking in deep water. *Annual Review of Fluid Mechanics*, (25), 373–397.

Basco, D.R. (1985). A qualitative description of wave breaking. *Journal of the Waterway Port Coastal and Ocean Engineering*, **3**(2), 171–188.

Battjes, J.A. (1974). Surf similarity. In: *Proceedings of the 14th conference on Coastal Engineering*, 1, 466–480.

Berthelsen, P.A. and Faltinsen, O.M. (2008). A local directional ghost cell approach for incompressible viscous flow problems with irregular boundaries. *Journal of Computational Physics*, **227**, 4354–4397.

Blenkinsopp, C. and Chaplin, J. (2008). The effect of relative crest submergence on wave breaking over submerged slopes. *Coastal Engineering*, **55**(12), 967–974.

Bonmarin, P. (1989). Geometric properties of deep-water breaking waves. *Journal of Fluid Mechanics*, **209**, 405–433.

Bradford, S.F. (2000). Numerical simulation of surf zone dynamics. *Journal of Waterway, Port, Coastal, and Ocean Engineering*, **126**(January/February), 1–13.

Chang, K.A., Hsu, T.J. and Liu, P.L.F. (2005). Vortex generation and evolution in water waves propagating over a submerged rectangular obstacle Part II: Cnoidal waves. *Coastal Engineering*, **52**(3), 257–283.

Chen, G., Kharif, C., Zaleski, S. and Li, J. (1999). Two-dimensional Navier-Stokes simulation of breaking waves. *Physics of Fluids*, **11**, 121–133.

Christensen, E.D. (1998). *Turbulence in breaking waves - a numerical investigation*. Ph.D. thesis, Technical University of Denmark.

Christensen, E.D. (2006). Large eddy simulation of spilling and plunging breakers. *Coastal Engineering*, **53**(5-6), 463–485. ISSN 03783839.

Christensen, E.D. and Deigaard, R. (2001). Large eddy simulation of breaking waves. *Coastal Engineering*, **42**, 53–86.

Cokelet, E. (1977). Breaking waves. *Nature*, **267**, 769–774.

Engsig-Karup, A.P. (2006). *Unstructured Nodal DG-FEM Solution of High-order Boussinesq-type Equations*. Ph.D. thesis, Technical University of Denmark, Lyngby.

Galvin, C.J. (1968). Breaker type classification on three laboratory beaches. *Journal of Geophysical Research*, **73**(12), 3651–3659. ISSN 01480227.

Gourlay, M.R. (1994). Wave transformation on a coral reef. *Coastal Engineerin*, **23**, 17–42.

Hieu, P.D., Katsutoshi, T. and Ca, V.T. (2004). Numerical simulation of breaking waves using a two-phase flow model. *Applied Mathematical Modelling*, **28**(11), 983–1005. ISSN 0307904X.

Ippen, A.T. and Kulin, G. (1954). The shoaling and breaking of the solitary wave. In: *Proceedings of the 5th conference on Coastal Engineering*, 27–47.

Iversen, H.W. (1952). Laboratory study of breakers. In: *Proceedings of the NBS Semicentennial Symposium on Gravity Waves, National Bureau of Standards Circular 521*, 9–32.

Iwagaki, Y. and Sakai, T. (1972). Shoaling of finite amplitude long waves on a beach of constant slope. In: *Proceedings of the 13th Conference on Coastal Engineering*, 347–364.

Iwata, K., Kawasaki, K. and Kim, D.S. (1996). Breaking limit, breaking and post-breaking wave deformation due to submerged structures. In: *Proceedings of the 24th Conference on Coastal Engineering*, 2338–2351.

Jacobsen, N.G., Fuhrman, D.R. and Fredsøe, J. (2012). A wave generation toolbox for the open-source CFD library : OpenFoam. *International Journal for Numerical Methods in Fluids*, **70**(November), 1073–1088.

Jiang, G.S. and Shu, C.W. (1996). Efficient implementation of weighted ENO schemes. *Journal of Computational Physics*, **126**, 202–228.

Kawasaki, K. and Iwata, K. (1998). Numerical analysis of wave breaking due to submerged breakewater in three-dimensional wave field. In: *Proceedings of the 26th conference on Coastal Engineering*, 853–866.

Kjeldsen, S.P. and Myrhaug, D. (1978). Kinematics and dynamics of breaking waves. Technical report, River and Harbour Laboratory (NHL), The Norwegian Institute of Technology.

Lader, P.F. (2002). *Geometry and Kinematics of Breaking Waves*. Ph.D. thesis, Norwegian University of Science and Technology.

Larsen, J. and Dancy, H. (1983). Open boundaries in short wave simulations - a new approach. *Coastal Engineering*, **7**, 285–297.

Lin, P. and Liu, P.L.F. (1998). A numerical study of breaking waves in the surf zone. *Journal of Fluid Mechanics*, **359**, 239–264.

Longuet-Higgins, M.S. and Cokelet, E.D. (1976). The deformation of steep surface waves on water I- A numerical method of computation. In: *Procedings of the Royal Society of London. Series A, Mathematical and Physical Sciences*, volume 350, 1–26.

Mayer, S., Garapon, A. and Sørensen, L.S. (1998). A fractional step method for unsteady free surface flow with applications to non linear wave dynamics. *International Journal for Numerical Methods in Fluids*, **28**, 293–315.

Miller, R. and Zeigler, J. (1964). The internal velocity field in breaking waves. In: *Coastal Engineering Proceedings*, 103–122.

Osher, S. and Sethian, J.A. (1988). Fronts Propagating with Curvature-Dependent Speed: Algorithms Based on Hamilton-Jacobi Formulations. *Journal of Computational Physics*, **79**, 12–49.

Peregrine, D.H. (1983). Breaking waves on beaches. *Annual Review of Fluid Mechanics*, (15), 149–178.

Perlin, M., Choi, W. and Tian, Z. (2013). Breakingwaves in deep and intermediate waters. *Annual Review of Fluid Mechanics*, (45), 115–145.

Rattanapitikon, W. and Shibayama, T. (2006). Breaking wave formulas for breaking depth and orbital to phase velocity ratio. *Coastal Engineering*, **48**(4), 395–416.

Sayce, A., Black, K. and Gorman, R. (1999). Breakingwave shape on surfing reefs. In: *Proceedings of Coasts and Ports '99, Perth, Australia*, 596–603.

Shu, C.W. and Osher, S. (1988). Efficient implementation of essentially non-oscillatory shock capturing schemes. *Journal of Computational Physics*, **77**, 439–471.

Smith, E.R. and Kraus, N.C. (1990). Laboratory study on macro-features of wave breaking over bars and artificial reefs. Technical report, Coastal Engineering Research Center.

Svendsen, I.A., Madsen, P.A. and Hansen, J.B. (1978). Wave Characteristics in the Surf Zone. In: *Proceedings of the coastal engineering conference*, 520–539.

Takikawa, K. and Yamada, F.and Matsumoto, K. (1997). Internal characteristics and numerical analysis of plunging breaker on a slope. *Coastal Engineering*, **31**(1), 143–161.

Ting, F.C.K. and Kim, Y.K. (1994). Vortex generation in water waves propagating over a submerged obstacle. *Coastal Engineering*, **24**(1), 23–49.

Tsai, C.P., Chen, H.B., Hwung, H.H. and Huang, M.J. (2005). Examination of empirical formulas for wave shoaling and breaking on steep slopes. *Ocean Engineering*, **32**(3-4), 469–483. ISSN 00298018.

van der Vorst H. (1992). Bi-CGSTAB: A fast and smoothly converging variant of Bi-CG for the solution of nonsymmetric linear systems. *SIAM Journal on scientific and Statistical Computing*, **13**, 631–644.

Vinje, T. and Brevig, P. (1981). Numerical simulation of breaking waves. *Advances in Water Resources*, **4**(2), 77–82.

Wang, Z., Yang, J., Koo, B. and Stern, F. (2009*a*). A coupled level set and volume-of-fluid method for sharp interface simulation of plunging breaking waves. *International Journal of Multiphase Flow*, **35**(3), 227–246.

Wang, Z., Zou, Q. and Reeve, D. (2009*b*). Simulation of spilling breaking waves using a two phase flow cfd model. *Computers and Fluids*, **38**(10), 1995–2005.

Yao, Y., Huang, Z., Monismith, S.G. and Lo, E.Y. (2013). Characteristics of monochromatic waves breaking over fringing reefs. *Journal of Coastal Research*, **29**(1), 94–104.

Zhao, Q., Armfield, S. and Tanimoto, K. (2004). Numerical simulation of breaking waves by a multi-scale turbulence model. *Coastal Engineering*, **51**(1), 53–80. ISSN 03783839.